Functional and Spectroscopic Measurements with Scanning Tunneling Microscopy

Amanda M. Moore and Paul S. Weiss

Departments of Chemistry and Physics, Pennsylvania State University, University Park, Pennsylvania 16802; email: stm@psu.edu

Annu. Rev. Anal. Chem. 2008. 1:857–82

The *Annual Review of Analytical Chemistry* is online at anchem.annualreviews.org

This article's doi:
10.1146/annurev.anchem.1.031207.112932

1936-1327/08/0719-0857$20.00

Key Words

STM manipulation, scanning tunneling spectroscopy, substrate-mediated interactions

Abstract

Invented as a surface analytical technique capable of imaging individual atoms and molecules in real space, scanning tunneling microscopy (STM) has developed and advanced into a technique able to measure a variety of structural, functional, and spectroscopic properties and relationships at the single-molecule level. Here, we review basic STM operation and image interpretation, techniques developed to manipulate single atoms and molecules with the STM to measure functional properties of surfaces, local spectroscopies used to characterize atoms and molecules at the single-molecule level, and surface perturbations affecting surface coverage and surface reactions. Each section focuses on determining the identity and function of chemical species so as to elucidate information beyond topography with STM.

STM: scanning tunneling microscopy

1. INTRODUCTION

The drive of analytical chemistry to measure compositions, morphologies, and concentrations of molecules from the bulk to the atomic scale has led to the development of techniques to characterize molecular and atomic arrangements on surfaces. Scanning tunneling microscopy (STM), invented by Binnig & Rohrer in 1981 (1) (and for which they won the Nobel prize in 1986), is able to determine atomic arrangements by rastering an atomically sharp tip across a flat conducting or semiconducting surface, thus rendering real-space images. This ability has made STM a widely used tool for surface characterization. Although many books (2–4) and reviews (5–7) have been written on STM development, theory, and use, the goal of this review is to focus on STM measurements beyond its most simple use as a real-space molecular and atomic probe. These measurements include the interpretation of STM images and the ability to manipulate single atoms and molecules, to obtain local spectroscopic data, and to characterize substrate-adsorbate interactions.

2. SCANNING TUNNELING MICROSCOPY OPERATION

An overview of STM operation is detailed schematically in **Figure 1**, which presents a one-dimensional metal-vacuum-metal STM tunnel junction. An atomically sharp conducting metal tip, typically tungsten or a platinum/iridium alloy, is brought within

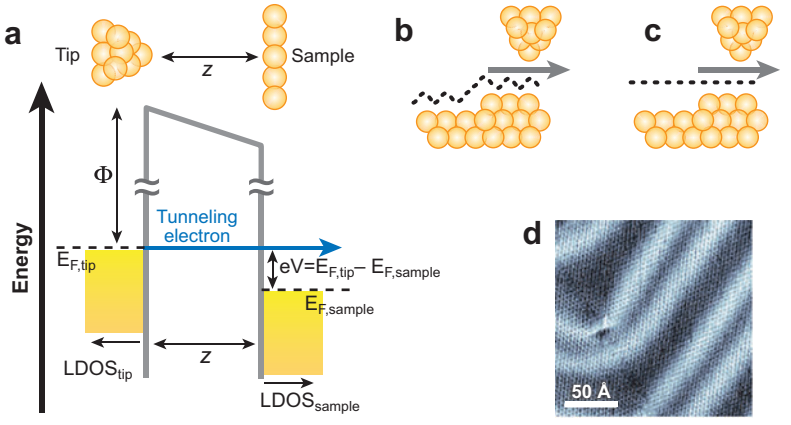

Figure 1

(*a*) An energy level diagram for a one-dimensional electron-tunneling junction. The Fermi energy levels (E_F) of the tip and sample are offset by the applied bias voltage (V) times the electron charge (e). The resultant current is exponentially dependent on the distance between the sample and the tip (*z*). LDOS, local density of states; Φ, work function of the metal. (*b*) Schematic of a scanning tunneling microscopy (STM) tip rastering across a metal surface in constant-current mode. The tip is extended and retracted, maintaining a constant tunneling current between tip and sample. (*c*) Schematic of a STM tip rastering across a metal surface in constant-height mode, maintaining a constant tip-sample separation, measuring current. (*d*) Atomically resolved topographic STM image operating in constant current mode of a Au{111} surface with herringbone reconstruction (95 Å × 95 Å $V_{sample} = -0.05$ V; $I_{tunnel} = 200$ pA).

a short distance (~3–10 Å) of a conducting or semiconducting sample using piezoelectric ceramic materials for probe tip placement and motion. An applied bias voltage (V) offsets the Fermi levels (E_F) of the tip and sample; the polarity of the bias voltage determines the direction of the electron flow. For instance, if $E_{F,tip}$ is greater than $E_{F,sample}$ (as shown in **Figure 1*a***), this shift allows electrons to tunnel from the occupied states of the tip into unoccupied states of the sample. By changing the bias polarity, electron flow occurs in the opposite direction (from sample to tip).

In classical mechanics, an electron traveling between the tip and the sample would require an energy greater than the work function of the tip/sample material to overcome the barrier between them. However, quantum-mechanically, electrons are able to tunnel across the barrier. The state of an electron in a one-dimensional junction with a rectangular barrier is

$$\psi(z) = \psi(0)e^{-\kappa z},$$

where

$$\kappa = \frac{\sqrt{2m(V-E)}}{\hbar},$$

ψ is the electronic wavefunction, z is the tip-sample separation, m is the electron mass, V is the potential in the barrier, E is the energy of the tunneling electron, and $\hbar$ is Planck's constant. Through the Born interpretation of the wavefunction, the square of the wavefunction is proportional to the probability distribution of the electron, and thus, the probability of tunneling yielding a tunneling current I:

$$|\psi(z)|^2 \propto e^{-2\kappa z} \propto I(z).$$

For small biases, the quantity (V-E) can be approximated as the work function (Φ) of the metal (~5 eV) (8); thus, the tunneling current decreases by about an order of magnitude for every 1-Å change in z. The molecular and atomic resolution of the STM is enabled through this exponential current decay; therefore, the tunneling current is extremely localized, and the STM is sensitive to both lateral and vertical changes in topography (often tenths of angstroms or less) (9, 10).

The STM tip is rastered across a surface in one of two modes: constant current (**Figure 1*b***) or constant height (**Figure 1*c***). In constant-current (the most common) mode, the feedback loop (FBL) maintains a set current by adjusting the tip-sample separation. The recorded topography is dependent on both the geometric structure and the local density of states (LDOS) of the tip and sample (9, 11, 12). Constant-current mode is able to measure surface features with higher precision (atomic resolution and better) as described above, but is generally slower due to the need for mechanical manipulation of the scanner in the z direction, controlled through the FBL. **Figure 1*d*** presents an atomic resolution image of a Au{111} herringbone–reconstructed substrate obtained in constant-current mode. In constant-height mode, the tip is maintained at a set distance from the sample during scanning, recording the current and allowing for much faster measurements; constant-height mode is most useful for relatively smooth surfaces.

Fermi level: the highest occupied electron energy state, where at 0 K no electrons will have enough energy to rise above this level

FBL: feedback loop

LDOS: local density of states

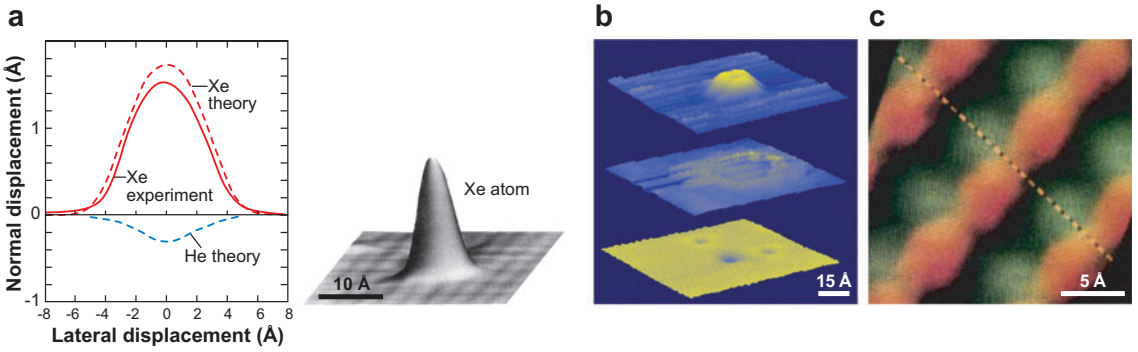

Figure 2

(*a*) (*Left*) Theoretically calculated apparent heights for Xe and He and experimentally measured apparent height for Xe. (*Right*) Scanning tunneling microscopy (STM) image of a Xe atom on Ni{110} (40 Å × 40 Å; $V_{sample} = -0.020$ V; $I_{tunnel} = 1$ nA). Adapted and reprinted with permission from References 11 and 13. Copyright 1991 and 1986, the American Physical Society. (*b*) STM images of Ni_3 clusters on MoS_2 (60 Å × 60 Å; V_{sample} from top to bottom: +2.0 V, +1.4 V, −2.0 V; I_{tunnel} from top to bottom: 100 pA, 100 pA, 200 pA). Reprinted with permission from Reference 16. Copyright 1998, the American Chemical Society. (*c*) Two superimposed STM images of GaAs{110}. Shown are the unoccupied states centered around the Ga atoms (false-colored *green*) and the occupied states centered around the As atoms (false-colored *red*). ($V_{sample} = +1.9$ and −1.9 V, recorded simultaneously.) Reprinted with permission from Reference 18. Copyright 1987, the American Physical Society.

Figure 2 illustrates systems wherein interpretation of the STM images depend upon the molecules present and the scanning conditions used to acquire the images, as STM images are a convolution of topography and electronic structure (LDOS). In the case of Xe adsorbed on Ni{110} (**Figure 2*a***), the most significant contribution to imaging at energies near the Fermi level is from the 6*s*-state of the adsorbate because the spatial extent is much larger for 6*s* than for 5*p*; the Lorentzian tail of each orbital crosses the Fermi level, although each is centered ∼4 eV away (11, 13, 14). Calculations of the LDOS (**Figure 2*a***, *left*) showed that for adsorbed He atoms, although they physically protrude from a surface, their apparent height in STM would be negative because He has a closed valence shell lower in energy and thus produces a decrease in the LDOS (13); this was confirmed experimentally (P.S. Weiss & D.M. Eigler, unpublished observations).

The location of an adsorbate on the surface and the STM tunneling conditions also influence the apparent height and shape of atoms at the surface at different adsorption sites (15, 16). As shown in **Figure 2*b***, a Ni_3 cluster was adsorbed on a MoS_2 surface and imaged at three sample bias voltages: +2.0 V, +1.4 V, and −2.0 V. At +2.0 V, the cluster appeared as a three-lobed protrusion, indicating that it enhanced the LDOS at this energy. When the sample bias was +1.4 V, the Ni_3 cluster did not appear as a protrusion from the MoS_2, but rather there appeared a diffuse ring resulting from a perturbation of the MoS_2 by the surface electronic structure of the cluster (17). At −2.0 V, the cluster appeared as a depression due to the depletion of the local density of filled states (16).

One of the most illuminating early examples of the convolution of topography and local electronic structure was found for images of GaAs(110). Here, Feenstra et al. showed that, depending on the bias voltage polarity, images of stoichiometric GaAs{110} surfaces display either the Ga atoms or the As atoms (18). **Figure 2*c*** is an overlay of two images acquired simultaneously at sample bias voltages of +1.9 V and −1.9 V. Calculations and electronegativity indicate that the unoccupied local state density is centered on the Ga atoms, whereas the occupied local state density is centered on the As atoms, consistent with their relative electronegativities (9, 18, 19).

Inelastic tunneling: tunneling between two states with different energies where energy is conserved through transfer, causing excitation (or deexcitation)

LM: lateral manipulation

VM: vertical manipulation

3. ATOM AND MOLECULE MANIPULATION

Manipulating atoms and molecules can lead to insights into surface properties and binding sites (20–24). Several methods have been developed to manipulate atoms and molecules using STM, including lateral, vertical, and inelastic tunneling–induced manipulation. Typically, manipulations are performed at low temperature and in vacuum (20–22, 25), although there are recent examples of large-molecule manipulation at room temperature in vacuum (26–29) and in liquid (30). Manipulation is a slow, serial process for building up structures, yet new and interesting phenomena have been discovered through manipulation.

3.1. Manipulation Types

The first example of STM manipulation was lateral manipulation (LM) used to move Xe atoms on metal surfaces (20, 21, 24); this technique has since been performed on many systems (23, 29, 31–40). The LM procedure consists of three steps. First, the probe tip is brought towards the surface, thereby increasing the tip-atom (tip-molecule) interaction. Second, the tip is moved to the desired location across the surface, thus moving the atom (molecule) under its influence. Finally, the tip is retracted, leaving the manipulated atom (molecule) at its final location on the surface (**Figure 3*a***, *top*) (31). Rieder and colleagues determined different modes of LM, measuring the tunneling current and feedback error signal during manipulation. These traces corresponded to: (1) pulling, where the STM tip is placed in front of the adatom, and the atom follows the tip due to an attractive tip-atom interaction; (2) pushing, where the atom or molecule is repelled and moves in front of the tip due to the interaction with the tip; and (3) sliding, where the atom or molecule is bound or trapped by the tip and moves along smoothly (shown schematically in **Figure 3*a***, *bottom*) (31).

A second manipulation technique transfers the atom or molecule vertically between the STM tip and the surface. Vertical manipulation (VM) (**Figure 3*b***, *top*) is performed by applying an electric field between the tip and sample when the tip is over the atom (molecule) to be moved, thus transferring the atom (molecule) to the STM tip. The tip is then moved to the new location and the electric field bias polarity is reversed, returning the atom (molecule) to the surface (21, 41–43). It is also possible to perform VM through mechanical contact, thereby picking up the atom or molecule with the tip (44, 45). **Figure 3*b***, *bottom* shows the current versus time plot for moving a Xe atom between the STM tip and a Ni{110} surface (41).

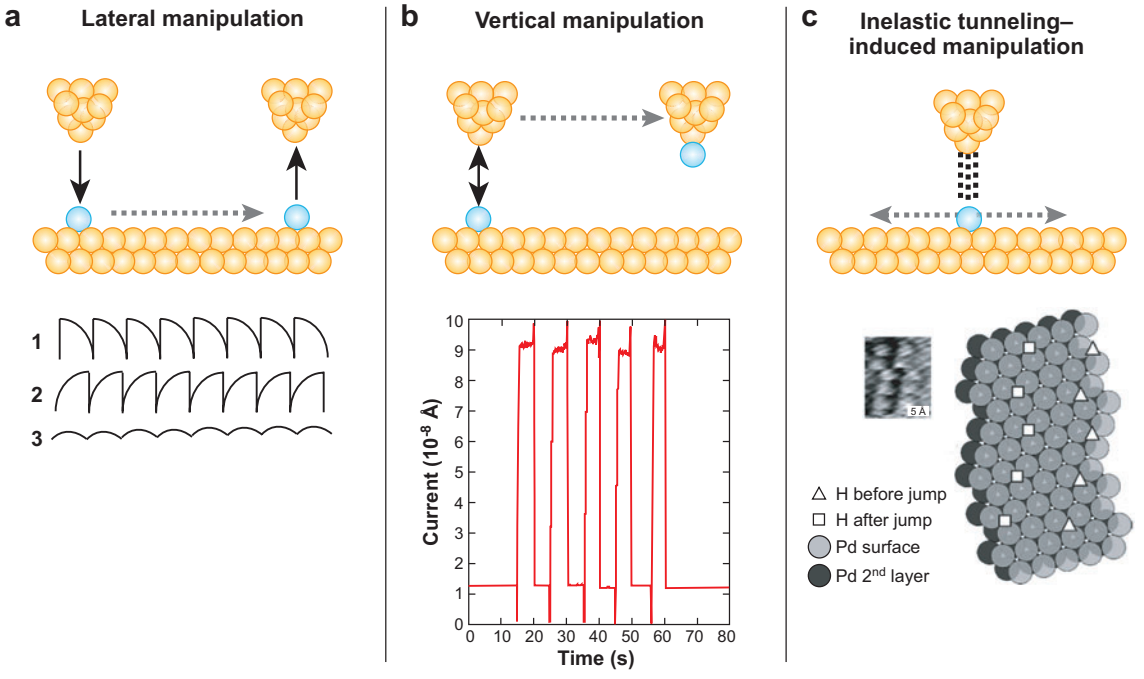

Figure 3

Uses of scanning tunneling microscopy (STM) to manipulate atoms and molecules. (*a*) Lateral manipulation, wherein the tip (1) pushes, (2) pulls, or (3) slides the manipulated species across the surface due to tip/sample interactions. (*b*) *Top*: Vertical manipulation, wherein the atom or molecule is vertically displaced by the STM tip. *Bottom:* Current versus time plot for picking up and replacing a Xe atom on a Ni{110} surface. Reprinted with the permission of Macmillan Publishers Ltd: *Nature* (41). Copyright 1991. (*c*) *Top*: Inelastic tunneling–induced manipulation, wherein tunneling electrons excite rotational, vibrational, or electronic transitions resulting in motion. *Bottom:* Hydrogen atoms manipulated through inelastic tunneling on a Pd surface. Reprinted with permission from Reference 49. Copyright 2006, American Chemical Society.

Inelastic electron tunneling (IET)–induced manipulation is a process wherein tunneling electrons or holes (depending on bias polarity) are injected from the tip positioned above the adsorbed atom (molecule), thus moving it (**Figure 3*c***, *top*). The electron energy is transferred through an excited state, leading to excitation (rotational, vibrational, or electronic), the rate of which is controlled by the applied bias and the tunneling current (33, 46–48). **Figure 3*c***, *bottom*, presents a schematic of H-atom manipulation on Pd{111} using IET (49, 50).

3.2. Functional Measurements Using Manipulation

IET: inelastic electron tunneling

Manipulation techniques have been used to study otherwise inaccessible systems by simply adsorbing molecules to surfaces. **Figure 4*a*** details how trajectories in LM are guided by the surface potential energy landscape on the atomic scale (40). In

this example, single Ag adatoms were manipulated on a Ag{111} surface at different angles (θ) relative to the close-packed [110] surface direction.

Moving atoms at a rate of 10 Å/s with a tunneling resistance of 15 kΩ for all motion, the small steps in the tip trace shown in **Figure 4*a*** indicate motion of the atom between face-centered cubic (fcc) and hexagonally close-packed (hcp) sites (*yellow arrows*), whereas larger steps (*white arrows*) indicate jumps from fcc to fcc (or hcp to hcp) sites due to tip motion away from the close-packed direction. When the angle from the close-packed direction is increased ($\theta = 20^\circ$), less time was spent traveling in the close-packed direction and the adatoms made larger jumps (*red arrows*) due to the surface corrugation. Prior to these larger jumps, the lateral force (seen in the tip traces) increased in order to give the atom enough energy to overcome the barriers to motion over the surface. Once the adatom hopped, the probe tip quickly retracted in response to the FBL. For $\theta = 30^\circ$ manipulation, the adatom did not travel along the close-packed direction; rather, theory predicted that the minimum energy path for this motion is to slide between threefold hollow sites around the surface atoms (*dotted white arrows*) (40, 51).

The LM for a single adatom described above involved sliding and slip-stick motions. Kelly, Tour, and colleagues have manipulated larger molecules known as nanocars, which contain fullerene (C_{60}) "wheels," and found that they roll across Au{111} surfaces (29). The chassis and axles of these nanocars were built from oligo(phenylene-ethynylene) (OPE) linkers and were attached to four fullerene wheels. The spacings between the fullerenes in the nanocars (each fullerene appeared as a protrusion) indicated the orientation of the car; the direction of travel was determined from sequences of images. **Figure 4*b*,*c*** displays STM images in which a single nanocar was manipulated by the STM tip. Only "pulling" motions (tip in front of the car) perpendicular to the axle direction moved the nanocar. Pushing the nanocar or pulling it in a direction parallel to the axles did not result in motion. By clever molecular design of three-fullerene molecules, Kelly, Tour, and colleagues determined that fullerene rotation (rather than sliding) was responsible for the motion of the nanocars (29).

In addition to building an understanding of motion on surfaces, VM has been used to change the LDOS of the tip, thus enhancing observation of the electronic properties. As the LDOS of the tip and sample are both important for STM imaging, VM has been used to attach molecules to an STM tip; using this assembly, surfaces can then be imaged, resolving surface structures not obtained from bare probe tips (45). Kelly et al. created fullerene-terminated STM tips by vacuum-depositing a fullerene film onto highly oriented pyrolytic graphite (HOPG), then bringing an STM tip (Pt:Rh) into contact with the film to lift a C_{60} molecule onto the tip. Using these functionalized tips, HOPG surfaces containing defects created by low-energy Ar^+ bombardment were imaged (**Figure 4*d***), revealing theoretically predicted (52) threefold scattering patterns and a $\sqrt{3} \times \sqrt{3}$ superlattice arising from the electrons scattering along hexagonal crystallographic directions of the two-dimensional graphite layers. At room temperature, these images were only observed using a fullerene-functionalized tip, effectively as a result of sharpening of the electronic structure of the tip, an effect that was reproduced with an unfunctionalized tip at 77 K (45, 53).

Electric field–induced manipulation has been useful not only for moving molecules from the surface to the tip or from one location to another, but also for changing the orientation of a molecule bound to a surface. We have studied functionalized OPE molecules inserted into host *n*-alkanethiolate and 3-mercapto-*N*-nonylpropionamide (1ATC9) matrices to understand how they function as conductance switches (54–60). In an *n*-alkanethiolate matrix, OPE molecules exhibit stochastic conductance switching between two conductance states (defined as ON and OFF), depending on the packing of the matrix around the inserted OPE molecules, and limited control was possible via the bias (54, 55). Nitro-functionalized OPE molecules were inserted into a 1ATC9 host containing buried hydrogen-bonding amide functionality, thus stabilizing the conductance states and enabling observations of switching

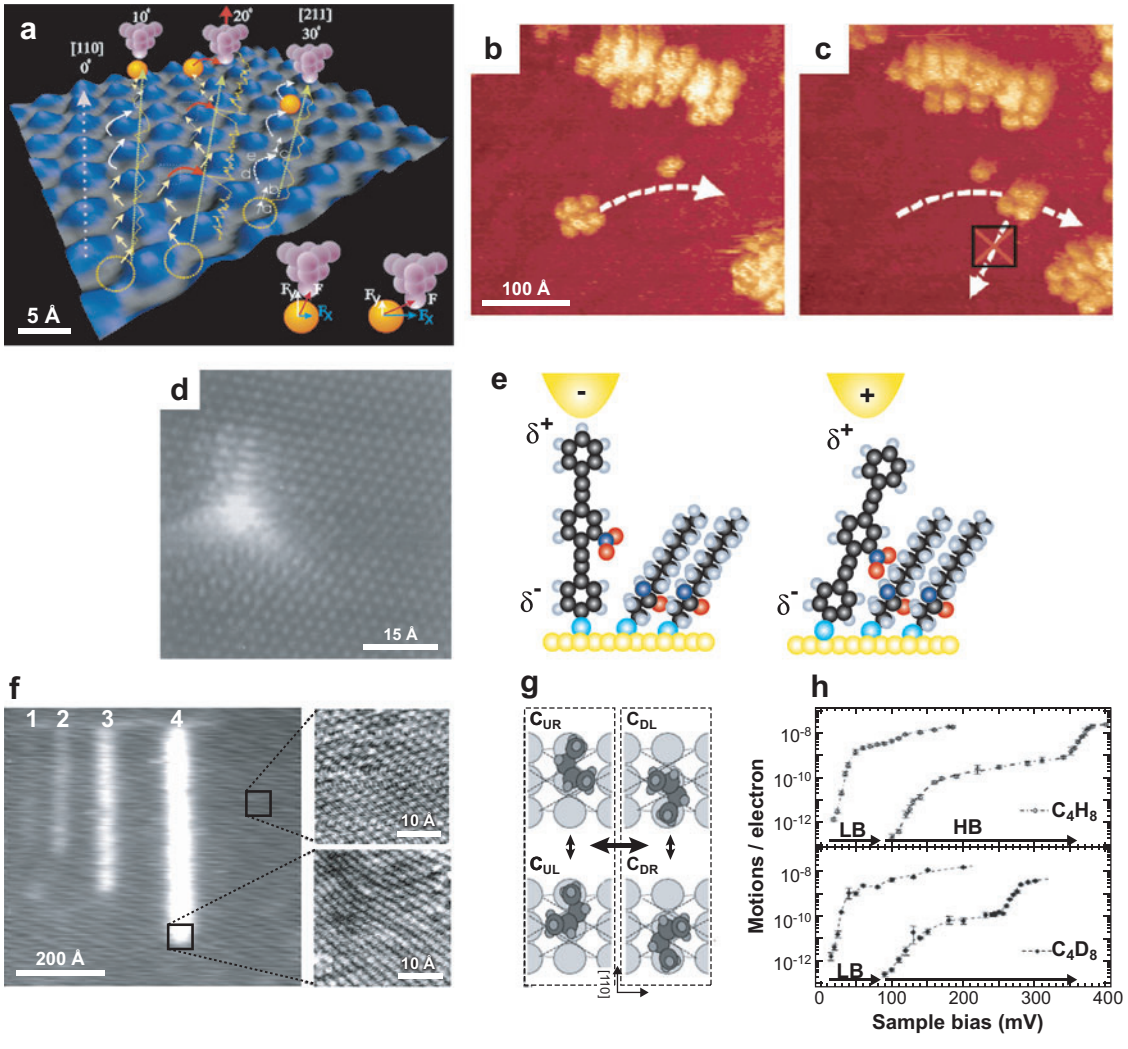

driven by the applied electric field between the STM tip and substrate. At positive sample bias, the nitro-functionalized OPE molecules were driven to the ON conductance state, and at negative sample bias, they were switched to the OFF conductance state (**Figure 4*e***). If the OPE molecules were not functionalized (i.e., did not contain the nitro-group on the middle phenylene ring), the bias polarity could not drive switching. We determined that the combination of the applied field interaction with the molecular dipole and the ability of the nitro-functionality to hydrogen-bond with the host matrix mediated the observed conductance switching. This was tested by designing molecules with a range of molecular dipole magnitudes and signs (56).

Depositing H_2 onto Pd{111} resulted in H atoms both adsorbed to the surface and absorbed into the bulk Pd (49, 50). **Figure 3*c*** illustrates how surface-adsorbed H can be manipulated using IET. Interestingly, the H atoms absorbed into the bulk Pd can be manipulated to just below the top layer of Pd using IET (**Figure 4*f***). The occupation of these sites was characterized using differential conductance imaging (described below). Differential conductance images recorded over bare Pd showed no distortion; however, when measured over the area patterned with subsurface H atoms, the hexagonal arrays of the surface Pd atoms were distorted (49, 50).

Action spectra can also be acquired using IET manipulation, shown experimentally using *cis*-2-butene (C_4H_8) (61). Here, Kawai and colleagues induced vibrationally

Figure 4

Examples of scanning tunneling microscopy (STM) lateral manipulation (LM) (*a-c*), vertical manipulation (VM) (*d-e*), and inelastic tunneling manipulation (*f*). (*a*) Superposition of an Ag{111} surface with tip-path manipulation signals. Lateral force components are shown (*bottom*, *right*). Also shown are the original positions of the adatoms (*dotted yellow circles*), the path of the tip motion (*dotted yellow lines*), the experimental tip path traces (*solid yellow lines*), and the hopping movements (*arrows*). See text for details. Reprinted with permission from Reference 40. Copyright 2003, the American Physical Society. (*b-c*) STM manipulation of a single nanocar (380 Å × 380 Å; $V_{sample} = 0.1$ V; $I_{tunnel} = 30$ nA; $I_{manipulation} = 3.5$ nA). The nanocar was pulled as indicated by the white arrow (*b*) to its location in panel *c*. The nanocar failed to move when the tip was moved 90° to the previous motion. Reprinted with permission from Reference 29. Copyright 2005, the American Chemical Society.
(*d*) STM image of a defect on highly oriented pyrolytic graphite (HOPG) imaged with a fullerene-functionalized tip (56 Å × 56 Å; $V_{sample} = -100$ mV; $I_{tunnel} = 1$ nA). Reprinted with permission from Reference 45. Copyright 1996, AAAS.
(*e*) Schematic of bias-controlled switching of nitro-functionalized oligo(phenylene-ethynylene) (OPE) molecules inserted into a 3-mercapto-*N*-nonyl-propionamide (1ATC9) host matrix using the STM electric field. (*f*) Manipulation of subsurface H atoms from the bulk Pd using STM at 4 K. (700 Å × 700 Å; $V_{sample} = 0.025$ V; $I_{tunnel} = 50$ pA.) The four lines were created by moving the tip over the surface at sample bias 0.7 V with currents of 1, 10, 50, and 150 pA for lines 1–4, respectively. The insets represent differential conductance images showing atomic resolution of the Pd{111} surface (30 Å × 30 Å; $V_{sample} = 0.018$ V; $I_{tunnel} = 200$ pA). *Top inset*: The hexagonal array of the Pd atoms over the surface was not distorted. *Bottom inset:* The hexagonal array is distorted over the patterned regions. Reprinted with permission from Reference 50. Copyright 2005, National Academy of Sciences, USA. (*g*) Proposed structural orientations of *cis*-2-butene on Pd{110}. (*h*) Action spectra for C_4H_8 (*top*) and C_4D_8 (*bottom*) ($I_{tunnel} = 3$ nA for C_4H_8 and 2 nA for C_4D_8). Reprinted with permission from Reference 61. Copyright 2005, the American Physical Society.

STS: scanning tunneling spectroscopy

mediated motion, moving the C_4H_8 between four equivalent orientations on Pd{110}. As shown in **Figure 4*g*** (*left*), motions between the pairs C_{UR} and C_{UL} or C_{DL} and C_{DR} were found to be low-barrier (LB) motions characterized by small changes in the tunneling current (<1 nA), whereas motions from one pair to the other pair were found to be high-barrier (HB) motions, with measured tunneling current changes of ~3 nA. Action spectra (**Figure 4*g***, *right*) with the motion yield (molecular motions per injected electron) as a function of sample bias were recorded for normal and deuterated (C_4D_8) *cis*-2-butene. Changes in the slopes of the action spectra indicated vibrational modes of the C_4H_8 molecules. The energies at the changes in the slope of the action spectra were compared with high-resolution electron energy loss spectroscopy (HREELS) data (62). From these data, the motion yields were assigned for the LB action spectra as the metal-carbon stretch for the C_4H_8 (C_4D_8) at ~37 mV (~31 mV) and for the C-H bending mode at ~115 mV (~95 mV) (with the expected isotopic shifts for the deuterated molecules). For the HB action spectra, the ~115 mV (~110 mV) was assigned as the C-C stretching mode, weakly influenced by the isotope effect, and the ~360 mV (~270 mV) was assigned as the C-H stretching mode. The carbon double-bond stretching mode was not visible in the action spectra.

4. SCANNING TUNNELING SPECTROSCOPY

Scanning tunneling spectroscopy (STS) has been used to characterize the electronic and vibrational properties of surfaces and adsorbed molecules. The advantage of STS lies in its ability to probe single atoms and molecules; however, it can be difficult to obtain STS spectra that are unaffected by outside influences. In many cases, STS measurements are taken in ultrastable instruments in ultrahigh vacuum (UHV) so as to isolate the sample from acoustic and vibrational noise; this is done at cryogenic temperatures to reduce the thermal spread of electron energies. To perform spectroscopy using the STM tunneling junction, the tunneling gap is typically held at a constant set point by interrupting the FBL while a voltage ramp is applied and the tunneling current is measured as a function of the applied bias voltage. The first and second derivatives of the conductance (*I/V*) can be measured using a lock-in amplifier (LIA); this results in differential conductance (*dI/dV*), which can be normalized to approximate the LDOS and inelastic scanning tunneling spectroscopy (d^2I/dV^2). The resulting peaks can sometimes be assigned as vibrational modes of adsorbed molecules, or for atomic-scale magnetic structures, they can be assigned as spin excitation spectra.

Early *I/V* measurements were performed on semiconducting surfaces (63–68). Conductance measurements were shown to depend on tip-sample separation (63, 64). Avouris and Lyo used this distance dependence to tune the interactions between tip and substrate, thereby gaining an understanding of reaction pathways for the oxidation of Si{111} 7 × 7 and manipulating adsorbates (63, 65). Further *I/V* measurements recorded over doped silicon surfaces displayed negative differential resistance over locations containing dopant molecules (66, 67).

Small changes in the slope of *I/V* spectra (**Figure 5*a***) arise from changes in the LDOS of the tip and sample and can be measured through the differential

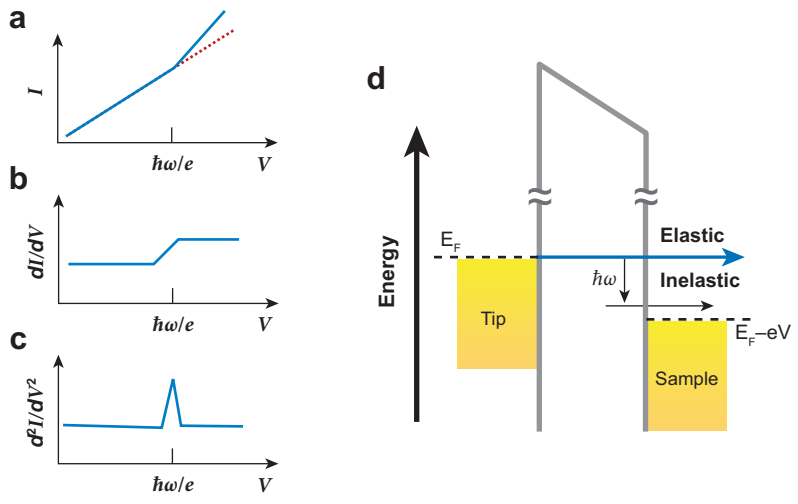

Figure 5

(*a*) Scanning tunneling spectroscopy (STS) for current versus voltage (I/V) measuring conductance. (*b*) Differential conductance (dI/dV) measuring the local density of states. (*c*) Inelastic STS (d^2I/dV^2) measuring molecular vibrations. (*d*) Energy level diagram for inelastic STS. When the electron energy rises above $\hbar\omega$, inelastic tunneling channels are accessible in the molecule, leading to molecular vibrations.

conductance (**Figure 5*b***). The current dependence on z may cause these features to be obscured, but they can be normalized using the ratio of the differential conductance to the (integral) conductance ($dI/dV/I/V$) (64, 69). Eigler and colleagues showed that for Fe adsorbed onto Pt{111} using three different tips, the normalized differential conductance spectra could be used to identify single Fe adatoms. The authors demonstrated this by acquiring spectra over both the Fe adatoms and the bare Pt{111}; peaks displayed in the Fe spectra and not the Pt{111} spectra were attributed to the Fe adatoms and were consistent with the expected state density (70).

Inelastic electron tunneling spectroscopy (IETS), measured as d^2I/dV^2 versus V spectra, produces vibrational spectra for molecules on surfaces. IETS spectra (**Figure 5*c***) are measured using phase-sensitive detection of the tunneling current at the second harmonic of the modulated bias voltage using a LIA (71–73). Such IETS spectra have been difficult to obtain due to the need for extreme mechanical stability to isolate the system acoustically and vibrationally (74), and for cryogenic temperatures to reduce the thermal spread of electronic energies (71–73). As shown schematically in **Figure 5*d***, the tunneling electrons lose energy ($\hbar\omega$) to vibrational modes of the molecules within the tunneling junction, giving rise to an inelastic tunneling channel. Examples include acetylene on Cu{100} (71), CO in constructed Fe(CO) species (72), and substrate-adsorbate vibrations for benzene on Ag{100} (73). Although IETS measurements for vibrational spectra have been performed, the selection rules and phase differences between elastic and inelastic channels are not yet understood (71–77). Furthermore, IETS measurements have been recorded for spin excitation spectra using a low-temperature UHV STM coupled with a high magnetic field. Tunneling electrons in this system lose energy to spin-flip excitations of single (or chains of) magnetic atoms within the tunneling junction with respect to the magnetic field applied to the sample (78–80).

IETS: inelastic electron tunneling spectroscopy

4.1. Scanning Tunneling Spectroscopy of Local Electronic Structure

With micro- and nanoelectronics reaching ever smaller scales, and with the ultimate limit of single molecules acting as electronic components, it has become important to measure and to compare the conductivities within and among families of single molecules. Highly conjugated molecules such as OPE molecules (described above) and oligo(phenylene-vinylene) (OPV) molecules have been of interest due to their potential use as molecular wires and switches (54, 55, 60, 81). Although the conductivities of alkanethiolates, OPEs, and OPVs can be measured as full monolayers (82–84), it is interesting to compare these measurements to the conductances of single molecules of the same species (81). Blum et al. used STS to measure the conductances of isolated α,ω-dithiols of dodecane, OPE, and OPV molecules inserted into host undecanethiolate monolayers. After insertion, the pendant thiols of the inserted molecules were exposed to solutions of gold nanoparticles, creating a second contact for each inserted molecule. Conductance measurements were obtained, showing that OPVs were the most conductive, followed by OPE molecules, with alkanethiolates the least conductive, thus scaling with bulk measurements over hundreds of molecules (81), consistent with electrochemical conductance measurements (85–87).

Ligand-stabilized metal nanoparticle systems represent another area in which charge transport dynamics are of interest (88–92). These systems, similar to the conductance measurements described above, contain a dithiol linker to tether a nanoparticle to a substrate. Isolated or tethered nanoparticles are able to exhibit single-electron transfer, and the energy required to add an extra electron to the particle is greater than k_BT, where k_B is Boltzmann's constant and T is absolute temperature (88, 93, 94). The energy required to charge a metallic nanoparticle with a single electron is inversely proportional to the particle's capacitance:

$$E_{charge} = \frac{e^2}{2C},$$

where $e = 1.602 \times 10^{-19}$ C. The particle's capacitance can be calculated as

$$C = 4\pi\varepsilon\varepsilon_0 r\,(1 + r/2L),$$

where ε is the dielectric constant of the ligand shell, ε_0 is the dielectric constant of vacuum, r is the radius of the particle, and L is the thickness of the tunneling junction (93–95).

A single nanoparticle addressed by STM can exhibit Coulomb blockade, which is the increase of the differential resistance near zero bias, and Coulomb staircase, which is quantized electron charging of the particle, both of which can be observed in the *I/V* spectra (89, 93–95). The potential around the Coulomb blockade region where current begins to flow is known as the threshold voltage. Coulomb blockade occurs in tunneling junctions and is described as resistor-capacitor circuits in series modeling two tunneling barriers controlling the electron transport through this junction; the first barrier is between the probe tip and the cluster, and the second barrier is between the cluster and the substrate. We have analyzed precise structures of isolated, ligand-stabilized undecagold clusters (Au_{11}) stabilized by triphenylphosphine ligands

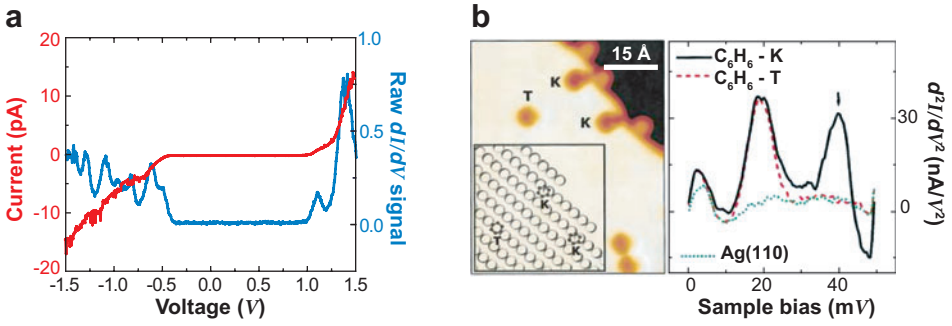

Figure 6

(*a*) Current versus voltage (*I/V*) exhibiting Coulomb blockade and differential conductance (*dI/dV*) displaying single-electron charging plots for a Au_{11} cluster bound to a Au{111} substrate via a decanedithiolate tether. Significant spectral diffusion is observed between spectra for these clusters. (*b*) *Left:* Scanning tunneling microscopy image of benzene adsorbed on Ag{110} (70 Å × 54 Å; $V_{sample} = 0.1$ V; $I_{tunnel} = 1.6$ nA). *Inset:* Model of the proposed location of the labeled molecules. *Right*: Inelastic scanning tunneling spectroscopy acquired over benzene molecules at K sites (*solid black line*), at T sites (*dotted red line*), and over the Ag{110} (*dotted green line*) ($V_{sample} = 0.1$ V; $I_{tunnel} = 2$ nA; $V_{AC} = 4$ mV rms at a frequency of 641 Hz). Reprinted with permission from Reference 73. Copyright 2001, the American Physical Society.

immobilized on octanethiolate self-assembled monolayers via α,ω-decanedithiolate tethers (89). Using ultrastable UHV STM operating at cryogenic temperatures, we were able to record high-resolution images as well as current-voltage and differential conductance spectra over the nanoparticle assemblies (**Figure 6*a***). Interestingly, for a single tethered Au_{11} cluster, as well as across many clusters, significant spectral diffusion was observed, including through the Coulomb blockade region. This study demonstrates that even in a well-defined, carefully controlled system, the electronic structure is still complex (89).

4.2. Scanning Tunneling Spectroscopy as a Local Vibrational Spectroscopy

Local vibrational spectroscopy was first demonstrated by Ho and colleagues, who measured isolated acetylene (C_2H_2) and deuterated acetylene (C_2D_2) on Cu{100} surfaces (71). They found a peak in the d^2I/dV^2 spectrum at 358 mV corresponding to the C-H stretching mode. Furthermore, taking vibrational spectra over the C_2D_2 resulted in the expected isotopic shift of the peak for the C-D stretching mode to 266 mV (71). The authors were also able to show hindered rotation of CO on Cu{100} and Cu{110} (76). They constructed mono- and dicarbonyl species of Fe on Ag{110} and measured the concomitant shifts in the C-O stretch for these species (72).

Rust and colleagues used IETS to study benzene molecules adsorbed to Ag{110} not only to identify the molecule on the surface, but to elucidate each molecule's chemical state and local environment. Using VM, benzene molecules were picked up

with the STM tip and imaging was performed with the tip-molecule system. Benzene molecules were found to be adsorbed to the Ag{110} surface at atop sites. Vibrational IETS spectra were recorded for isolated chemisorbed benzene molecules on terraces and at step edges, as well as for benzene adsorbed as a dense hexagonally packed ordered monolayer, which hindered lateral movement of the benzene molecules. For isolated benzene on a terrace, IETS peaks appeared at 4 and 19 mV due to excitation of adsorbate-substrate vibrational modes. When the benzene molecules were hexagonally packed, these peaks shifted to 7 and 44 mV, showing that IETS is sensitive to the chemical environment of the adsorbate. Furthermore, when comparing IETS spectra of molecules adsorbed on a terrace (T) to spectra of molecules adsorbed near a substrate step edge (K), the latter exhibited an additional peak at 39 mV, a vibration not visible at other sites. In the STM images (**Figure 6*b***), molecules adsorbed at the K sites had an asymmetric shape due to their interactions with nearby kink sites, which was believed to contribute to the additional vibrational peak (73).

4.3. Scanning Tunneling Spectroscopy of Local Magnetic Structure

To record spin-excitation spectra, Mn atoms were adsorbed to NiAl(110) surfaces containing Al_2O_3 islands (78). Differential conductance spectra were recorded over the individual Mn atoms. After applying a magnetic field, the Mn adsorbed on the oxide islands exhibited a dip in the differential conductance spectra centered at zero bias. The Al_2O_3 insulation layer was necessary to isolate the Mn atoms from the conducting surface for the IETS spectra to be observed. The IETS spin-flip signature was observed as a step in the *dI/dV* spectra corresponding to the spin-flip transistion. The observed conductance steps shifted to higher energy with increased magnetic field strength (78).

Further experiments used STM manipulation to create linear chains of 1 to 10 Mn atoms over which IETS spin-excitation spectra were recorded (79). In this study, the Mn atoms were deposited on a Cu{100} surface containing insulating islands of copper nitride. The *dI/dV* spectra recorded for the chains displayed dependence on the parity of the chains (i.e., odd-length chains exhibited a dip around zero bias, whereas this dip was absent from the even-length chain spectra). A spin-flip excitation required a total spin greater than zero, which was available in the odd-length chains. In the even-length chains, however, the ground state spin was zero. Both odd- and even-length chains displayed steps in the *dI/dV* spectra at larger energies. These steps corresponded to the spin-changing transitions from the ground state (singlet) to an excited state (triplet) (79).

In addition to the Mn chains, individual Fe and Mn atoms were deposited on CuN islands on Cu{100} to determine the magnetic anisotropy of single atomic spins (80). For Fe atoms at zero-field, a strong excitation was observed, indicating strong magnetic anisotropy in the system—stronger than that observed for the Mn atoms. Using STM manipulation, the Fe and Mn atoms were positioned so that the magnetic field was oriented along two different spatial directions. The excitation energies for the spectral steps changed depending on the binding site location, and the Fe and Mn atoms could be manipulated between the two binding sites, thereby

switching between the excitation spectra. The dependence of the spin excitations on the field direction represented further evidence of strong magnetic anisotropy (80).

5. SUBSTRATE-MEDIATED INTERACTIONS

An important and beautiful aspect of STM is that it can be used to image specific empty and filled orbitals in much the way that a mobile adsorbate might "see" them. This enables one to probe the local electronic structures that drive the chemistry, dynamics, and other surface processes. Substrate-mediated interactions have been shown theoretically and experimentally to influence adsorbate bonding and dynamics at ranges far beyond chemical bonding distances (96–98). Surface-state electrons of close-packed surfaces of noble metals are known to behave as two-dimensional electron gases (99–101). These surface-state electrons are scattered by substrate steps, defects, and adsorbates, creating standing waves that can mediate interactions between adsorbates (17, 102–110). Here, we describe how the STM is used to map these electronic perturbations and how they are used to understand reactions and motion at the single-molecule level.

5.1. Surface Electronic Structure Perturbation

Figure 7 illustrates three ways in which the electronic structure of a surface may be perturbed. The strongest of these (**Figure 7*a***), known as the Smoluchowski effect, occurs at substrate step edges, where the electron distribution at the step is smoothed by a charge transfer from the top to the bottom of the step edge (111). This effect is illustrated in **Figure 7*a*** (*bottom*), wherein benzene molecules are shown to have adsorbed in two rows, one at the top and one at the bottom of a Cu{111} step at 77 K (102, 105). A second, intermediate effect (**Figure 7*b***) is the adsorption of atoms on the surface perturbing the local surface electronic structure (15, 102, 104, 105). The STM image (**Figure 7*b***, *bottom*) shows an isolated benzene molecule on Pt{111}. The LDOS surrounding this molecule is perturbed several substrate lattice sites away from the molecule. Note that this effect is also seen in **Figure 7*a*** (*bottom*), where these local perturbations constructively and destructively interfere. The third and weakest effect (**Figure 7*c***, *top*) on the electronic structure is the scattering of surface-state electrons from features such as step edges, surface defects, and adsorbates (**Figure 7*c***, *bottom*) with scattering from Br islands on Cu{111} (99, 102, 112–114).

Electronic structures are imaged with STM at biases close to the Fermi level or through differential conductance imaging. At low biases, the STM images approximate the LDOS at the Fermi level (9, 99). Using dI/dV imaging, the Avouris and Eigler groups found that the wavelength of the oscillation in the surface LDOS changed as a function of energy; they subsequently mapped the (previously known) dispersion curves (99, 113).

Lau and Kohn theoretically predicted that long-range interactions were mediated by partially filled surface-state bands leading to oscillatory interaction potentials, known as Friedel oscillations, with periods of half the Fermi wavelength ($\lambda_F/2$) of the substrate (115). These results were initially confirmed with field ion microscopy (97).

Friedel oscillations: the distribution of electrons around a surface impurity

Fermi wavelength: the wavelength of the carriers that dominate electrical transport

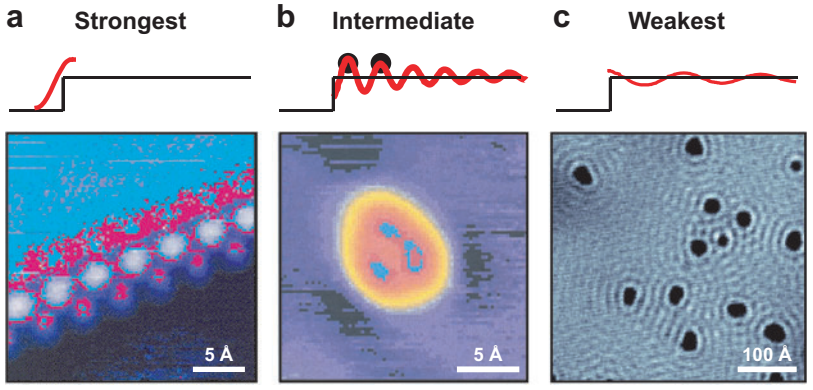

Figure 7

Substrate-mediated interactions on surfaces. (*a*) The strongest interactions occur at step edges where the electron distribution is smoothed by a charge transfer from the top to the bottom of the step edge. The scanning tunneling microscopy (STM) image shows benzene on Cu{111} (30 Å × 30 Å; $V_{sample} = 100$ mV; $I_{tunnel} = 100$ pA). Reprinted with permission from Reference 17. Copyright 2003, the American Chemical Society. (*b*) An intermediate substrate-mediated interaction occurs when atoms adsorb onto a surface, perturbing the local surface electronic structure. The STM image shows a single benzene atom as a three-lobed feature on Pt{111} with local electronic perturbations, imaged as depressions along the direction of the lobes of the benzene molecules (20 Å × 20 Å; $V_{sample} = 0.05$ V; $I_{tunnel} = 100$ pA). Reprinted with permission from Reference 15. Copyright 1993, the American Physical Society. (*c*) The weakest of the substrate-mediated interactions is the scattering of the electrons in the surface state from surface features such as step edges. The STM image shows Br adatom islands (*depressions*) on Cu{111} with local electronic perturbations imaged close to the Fermi level (420 Å × 420 Å; $V_{sample} = -50$ mV; $I_{tunnel} = 20$ pA). Reprinted with permission from Reference 104. Copyright 2007, the American Physical Society.

Later, with STM, single adatoms of Cu and Co were studied for their contributions to Friedel oscillations; it was found that the substrate surface-state electrons were most important to long-range interactions, as opposed to the identity of the adsorbate (109, 110). The coherence length (λ_C) for the surface-state electron standing wave pattern is inversely proportional to the temperature (T) of the surface and can be calculated using the following equation:

$$\lambda c \cong \frac{\hbar^2 k_F}{3.5 m^* k_B T},$$

where k_F is the Fermi level wave vector of the surface state, k_B is Boltzmann's constant, and m^* is the effective mass of a surface-state electron (116, 117). This yields an estimate of the distance at which molecules can communicate across a surface.

Coherence length: the propagation distance over which a wave maintains its ability to exhibit interference

5.2. Substrate-Mediated Interactions between Adsorbed Molecules

The high symmetry, relatively simple electronic structure, and high STM contrast resolution of benzene have made it a useful probe molecule for studying

substrate-adsorbate interactions (73, 102, 105, 118, 119). At low temperatures, the rate of diffusion for benzene molecules can be lowered sufficiently for individual molecules to be observed. Isolated benzene adsorbed on Pt{111} displays three distinct molecular shapes, which are attributed to benzene lying flat at three different surface sites and are due to changes in the interactions between the adsorbed molecules and the surface electronic states (15, 120). As shown in **Figure 7*a***, when benzene is adsorbed on Cu{111} it decorates both the tops and bottoms of monatomic step edges, perturbing the surface electronic structure and thereby setting up adsorption sites for subsequent rows of molecules (102, 105). When a higher coverage of benzene is deposited on the Cu{111} surface and the bias voltage is increased, the STM tip sweeps benzene from the terrace to the step, resulting in the third and fourth "phantom" rows observed in the STM images (**Figure 8*a***). These rows appear noisy in STM images, indicating that benzene molecules diffuse into and out of, or between, binding sites created by the adsorption of the first row of molecules. This diffusion occurs faster than the time scale of the STM images (17, 105). Benzene adsorbed on Au{111} at low coverage (0.1 monolayer) shows adsorption only at surface defect sites and at the top of Au{111} step edges, indicating that benzene seeks areas of high empty-state density, consistent with its nucleophilicity (121). Finally, if benzene is adsorbed on Ag{110} at low coverage, molecules only adsorb at the [1$\bar{1}$0] step edges (**Figure 8*b***) (73, 118, 122) due to the necessity of available free charge and free sites for the charge to occupy. For Ag{110}, anisotropy exists in the bulk density of states leading to reduction in the charge transfer for [001] steps, thereby reducing the ability of the step sites to accept charge from the benzene (123). Only the [1$\bar{1}$0] steps, which are the ends of silver closed-packed atomic rows, allow adsorption (122).

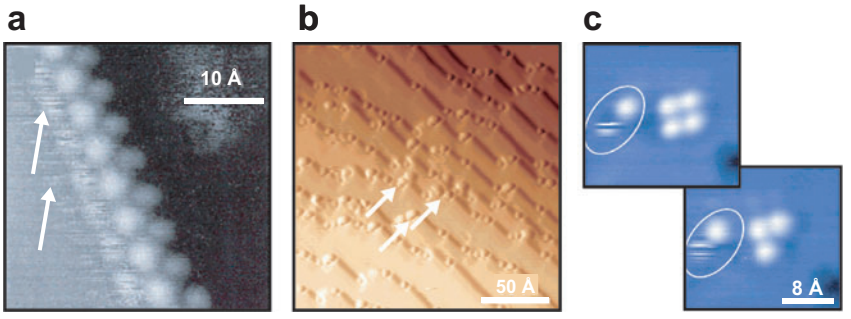

Figure 8

(*a*) Scanning tunneling microscopy (STM) image of benzene adsorbed at a Cu{111} step edge. The STM tip has moved additional benzene molecules to the second and third rows above the step (*white arrows*) (V_{sample} = 100 mV; I_{tunnel} = 100 pA). Reprinted with permission from Reference 105. Copyright 1995, Elsevier. (*b*) STM image of benzene deposited on Ag{110} at 66 K. Benzene molecules adsorb only on the [1$\bar{1}$0] step edges (*white arrows*) (V_{sample} = 0.05 V; I_{tunnel} = 4 nA). Reprinted with permission from Reference 17. Copyright 2003, the American Chemical Society. (*c*) STM images showing clusters of phenyl intermediates on Cu{111} at 77 K (V_{sample} = 200 mV; I_{tunnel} = 80 pA). Reprinted with permission from Reference 17. Copyright 2003, the American Chemical Society.

The surface-catalyzed formation of biphenyl from halobenzene molecules adsorbed on Cu{111} proceeds through a series of steps. First, the halobenzene (e.g., C_6H_5Br, C_6H_5I) adsorbs on the copper surface, dissociating above 180 K to form surface-bound halogen atoms and phenyl intermediates (124). Between 180 K and 300 K, the phenyl groups diffuse on the surface and above 300 K they react, forming biphenyl. Rieder and colleagues used manipulation techniques to control the dissociation, position, orientation, and coupling of iodobenzene molecules adsorbed adjacent to Cu{111} steps in each step of the reaction (125). We exposed a Cu{111} crystal to iodobenzene at 293 K, then cooled the crystal to 77 K for STM measurements (119). At this temperature, phenyl binds to both step edges and at terrace sites with moderate diffusion on open terraces. Phenyl pairs are observed to form and to break, as shown in **Figure 8*c***. This indicates relatively weak intermolecular interactions and suggests that the intermediates have not coupled to form covalent bonds. The geometry of the dimer indicates that the phenyl unsatisfied bonds are facing either towards or away from one another. The role of the substrate-mediated interaction is twofold: The surface is needed to create the phenyl intermediates and the phenyl species on the surface experience intermolecular forces due to loosely bound complexes that position the phenyl intermediates in close proximity and prealign them for the reaction to form biphenyl.

The atomic halide intermediates in this reaction were also studied (104). In this experiment, bromobenzene was adsorbed to a Cu{111} surface at 293 K, and Br adatom islands were formed by ramping the substrate temperature to 600 K. At 4 K, the standing wave interference patterns of the surface state scattering from the Br adatom islands were imaged using STM, and the long-range interactions were quantified by determining the interisland distances. The interaction potential (E_r) between the islands was determined as

$$E_r = -k_B T \ln[(g(r))],$$

where k_B is Boltzmann's constant, T is the temperature at which the islands were formed, and $g(r)$ is the pair correlation function, which was extracted by dividing the experimental pair distribution function by the theoretical function for similar noninteracting species. The coherence length of the Cu was calculated to be ~22 Å, which is consistent with the elevated temperature at which the Br atoms are mobile and form islands. This analysis showed the oscillations in the interisland distance interaction potential to have a periodicity of ($\lambda_F/2$) of Cu{111} up to a distance of ~56 Å (104).

6. CONCLUSIONS AND FUTURE PROSPECTS

STM has been developed into an analytical technique not only capable of imaging compositions and structures at surfaces, but also useful for understanding binding sites and reaction processes. Here, we have presented an overview of STM image interpretation, STM atom and molecule manipulation, STS, and substrate-mediated interactions. Future work will soon make STM an even more powerful analytical

technique by simultaneously coupling secondary signals, including photons and microwaves, into and out of the STM tunneling junction (126–130). Early results in these areas bode well for future applications of STM.

SUMMARY POINTS

1. STM images are a convolution of topography and electronic structure, which must be understood in order to interpret images.
2. Atomic and molecular manipulations can be used to elucidate the properties of a surface and adsorbates including the electronic structure and the vibrational modes of molecules at the surface.
3. STS gives insights into the conductances of molecules, the LDOS of the surface and adsorbates, and the vibrational modes of molecules.
4. Substrate-mediated interactions modulate adsorbate potentials, determine adsorption sites, and guide adsorbates and reaction pathways for catalytic reactions.

FUTURE ISSUES

1. Selection rules for IETS are still being determined.
2. Coupling secondary signals into the scanning tunneling microscope tunneling junction will lead to unprecedented abilities to characterize systems at the single-molecule level.

DISCLOSURE STATEMENT

The authors are not aware of any biases that might be perceived as affecting the objectivity of this review.

ACKNOWLEDGMENTS

The authors gratefully acknowledge support from the Air Force Office of Scientific Research, the Army Research Office, the Defense Advanced Research Projects Agency, the National Institutes for Standards and Technology, the National Science Foundation, and the Office of Naval Research.

LITERATURE CITED

1. Binnig G, Rohrer H, Gerber C, Weibel E. 1982. Surface studies by scanning tunneling microscopy. *Phys. Rev. Lett.* 49:57–61
2. Bonnell DA, ed. 2001. *Scanning Probe Microscopy and Spectroscopy: Theory, Techniques, and Applications*. New York: Wiley

3. Chen CJ. 1993. *Introduction to Scanning Tunneling Microscopy*. New York: Oxford Univ. Press
4. Stroscio JA, Kaiser WJ. 1993. *Scanning Tunneling Microscopy*. San Diego: Academic
5. Binnig G, Rohrer H. 1986. Scanning tunneling microscopy. *IBM J. Res. Develop.* 30:355–69
6. Binnig G, Rohrer H. 1987. Scanning tunneling microscopy: from birth to adolescence. *Rev. Mod. Phys.* 59:615–25
7. Griffith JE, Kochanski GP. 1990. Scanning tunneling microscopy. *Annu. Rev. Mater. Sci.* 20:219–44
8. Coombs JH, Welland ME, Pethica JB. 1988. Experimental barrier heights and the image potential in scanning tunneling microscopy. *Surf. Sci.* 198:L353–58
9. Tersoff J, Hamann DR. 1985. Theory of the scanning tunneling microscope. *Phys. Rev. B* 31:805–13
10. Garcia N. 1986. Theory of scanning tunneling microscopy and spectroscopy: resolution, image and field states, and thin oxide layers. *IBM J. Res. Develop.* 30:533–42
11. Eigler DM, Weiss PS, Schweizer EK. 1991. Imaging Xe with a low-temperature scanning tunneling microscope. *Phys. Rev. Lett.* 66:1189–91
12. Tersoff J, Hamann DR. 1983. Theory and application for the scanning tunneling microscope. *Phys. Rev. Lett.* 50:1998–2001
13. Lang ND. 1986. Theory of single-atom imaging in the scanning tunneling microscope. *Phys. Rev. Lett.* 56:1164–67
14. Lang ND. 1987. Apparent size of an atom in the scanning tunneling microscope as a function of bias. *Phys. Rev. Lett.* 58:45–48
15. Weiss PS, Eigler DM. 1993. Site dependence of the apparent shape of a molecule in scanning tunneling microscope images: benzene on Pt{111}. *Phys. Rev. Lett.* 71:3139–42
16. Kushmerick JG, Weiss PS. 1998. Mobile promoters on anisotropic catalysts: nickel on MoS_2. *J. Phys. Chem. B* 102:10094–97
17. Sykes ECH, Han P, Kandel SA, McCarty GS, Weiss PS. 2003. Substrate-mediated interactions and intermolecular forces between molecules adsorbed on surfaces. *Acc. Chem. Res.* 36:945–53
18. Feenstra RM, Stroscio JA, Tersoff J, Fein AP. 1987. Atom-selective imaging of the GaAs(110) surface. *Phys. Rev. Lett.* 58:1192–95
19. Lubinsky AR, Duke CB, Lee BW, Mark P. 1976. Semiconductor surface reconstruction: the rippled geometry of GaAs(110). *Phys. Rev. Lett.* 36:1058–61
20. Weiss PS, Eigler DM. 1992. Adsorption and accommodation of Xe on Pt{111}. *Phys. Rev. Lett.* 69:2240–43
21. Weiss PS, Eigler DM. 1993. What is underneath? Moving atoms and molecules to find out. In *NATO ASI Series E: Applied Sciences*, ed. T Binh, N Garcia, K Dransfeld, 213–17. Amsterdam: Kluwer Academic
22. Hla SW. 2005. Scanning tunneling microscopy single atom/molecule manipulation and its application to nanoscience and technology. *J. Vac. Sci. Technol. B* 23:1351–60

23. Manoharan HC, Lutz CP, Eigler DM. 2000. Quantum mirages formed by coherent projection of electronic structure. *Nature* 403:512–15
24. Eigler DM, Schweizer EK. 1990. Positioning single atoms with a scanning tunneling microscope. *Nature* 344:524–26
25. Jensen SC, Baber AE, Tierney HL, Sykes ECH. 2007. Adsorption, interaction, and manipulation of dibutyl sulfide on Cu{111}. *ACS Nano* 1:22–29
26. Cuberes MT, Schlittler RR, Gimzewski JK. 1996. Room-temperature repositioning of individual C_{60} molecules at Cu steps: operation of a molecular counting device. *Appl. Phys. Lett.* 69:3016–18
27. Jung TA, Schlittler RR, Gimzewski JK, Tang H, Joachim C. 1996. Controlled room-temperature positioning of individual molecules: molecular flexure and motion. *Science* 271:181–84
28. Sloan PA, Palmer RE. 2005. Two-electron dissociation of single molecules by atomic manipulation at room temperature. *Nature* 434:367–71
29. Shirai Y, Osgood AJ, Zhao Y, Kelly KF, Tour JM. 2005. Directional control in thermally driven nanocars. *Nano Lett.* 5:2330–34
30. Griessl SJH, Lackinger M, Jamitzky F, Markert T, Hietschold M, et al. 2004. Room-temperature scanning tunneling microscopy manipulation of single C-60 molecules at the liquid-solid interface: playing nanosoccer. *J. Phys. Chem. B* 108:11556–60
31. Bartels L, Meyer G, Rieder KH. 1997. Basic steps of lateral manipulation of single atoms and diatomic clusters with a scanning tunneling microscope tip. *Phys. Rev. Lett.* 79:697–700
32. Gross L, Moresco F, Alemani M, Tang H, Gourdon A, et al. 2003. Lander on Cu(211)-selective adsorption and surface restructuring by a molecular wire. *Chem. Phys. Lett.* 371:750–56
33. Hla SW, Braun KF, Wassermann B, Rieder KH. 2004. Controlled low-temperature molecular manipulation of sexiphenyl molecules on Ag(111) using scanning tunneling microscopy. *Phys. Rev. Lett.* 93:208302
34. Joachim C, Tang H, Moresco F, Rapenne G, Meyer G. 2002. The design of a nanoscale molecular barrow. *Nanotechnology* 13:330–5
35. Lagoute J, Kanisawa K, Fölsch S. 2004. Manipulation and adsorption-site mapping of single pentacene molecules on Cu(111). *Phys. Rev. B* 70:245415
36. Meyer G, Zöphel S, Rieder KH. 1996. Scanning tunneling microscopy manipulation of native substrate atoms: a new way to obtain registry information on foreign adsorbates. *Phys. Rev. Lett.* 77:2113–16
37. Moresco F, Meyer G, Rieder KH, Tang H, Gourdon A, et al. 2001. Recording intramolecular mechanics during the manipulation of a large molecule. *Phys. Rev. Lett.* 87:088302
38. Stroscio JA, Celotta RJ. 2004. Controlling the dynamics of a single atom in lateral atom manipulation. *Science* 306:242–47
39. Stroscio JA, Eigler DM. 1991. Atomic and molecular manipulation with the scanning tunneling microscope. *Science* 254:1319–26
40. Hla SW, Braun KF, Rieder KH. 2003. Single-atom manipulation mechanics during a quantum corral construction. *Phys. Rev. B* 67:201402

41. Eigler DM, Lutz CP, Rudge WE. 1991. An atomic switch realized with the scanning tunneling microscope. *Nature* 352:600–3
42. Bartels L, Meyer G, Rieder KH. 1997. Controlled vertical manipulation of single CO molecules with the scanning tunneling microscope: a route to chemical contrast. *Appl. Phys. Lett.* 71:213–15
43. Bartels L, Meyer G, Rieder KH. 1998. Dynamics of electron-induced manipulation of individual CO molecules on Cu(111). *Phys. Rev. Lett.* 80:2004–7
44. Dujardin G, Mayne A, Robert O, Rose F, Joachim C, et al. 1998. Vertical manipulation of individual atoms by a direct STM tip-surface contact on Ge(111). *Phys. Rev. Lett.* 80:3085–88
45. Kelly KF, Sarkar D, Hale GD, Oldenburg SJ, Halas NJ. 1996. Threefold electron scattering on graphite observed with C_{60}-adsorbed STM tips. *Science* 273:1371–73
46. Komeda T, Kim Y, Kawai M, Persson BNJ, Ueba H. 2002. Lateral hopping of molecules induced by excitation of internal vibration mode. *Science* 295:2055–58
47. Lauhon LJ, Ho W. 2000. Control and characterization of a multistep unimolecular reaction. *Phys. Rev. Lett.* 84:1527–30
48. Stipe BC, Rezaei MA, Ho W. 1997. Single-molecule dissociation by tunneling electrons. *Phys. Rev. Lett.* 78:4410–13
49. Fernández-Torres LC, Sykes ECH, Nanayakkara SU, Weiss PS. 2006. Dynamics and spectroscopy of hydrogen atoms on Pd{111}. *J. Phys. Chem. B* 110:7380–84
50. Sykes ECH, Fernández-Torres LC, Nanayakkara SU, Mantooth BA, Nevin RM, et al. 2005. Observation and manipulation of subsurface hydride in Pd{111} and its effect on surface chemical, physical and electronic properties. *Proc. Natl. Acad. Sci.* 102:17907–11
51. Kühnle A, Meyer G, Hla SW, Rieder KH. 2002. Understanding atom movement during lateral manipulation with the STM tip using a simple simulation method. *Surf. Sci.* 499:15–23
52. Mizes HA, Foster JS. 1989. Long-range electronic perturbations caused by defects using scanning tunneling microscopy. *Science* 244:559–62
53. Kushmerick JG, Kelly KF, Rust H-P, Halas NJ, Weiss PS. 1999. Observations of anisotropic electron scattering on graphite with a low-temperature scanning tunneling microscope. *J. Phys. Chem. B* 103:1619–22
54. Donhauser ZJ, Mantooth BA, Kelly KF, Bumm LA, Monnell JD, et al. 2001. Conductance switching in single molecules through conformational changes. *Science* 292:2303–07
55. Donhauser ZJ, Mantooth BA, Pearl TP, Kelly KF, Nanayakkara SU, et al. 2002. Matrix-mediated control of stochastic single molecule conductance switching. *Jpn. J. Appl. Phys.* 41:4871–77
56. Lewis PA, Inman CE, Maya F, Tour JM, Hutchison JE, et al. 2005. Molecular engineering of the polarity and interactions of molecular electronic switches. *J. Am. Chem. Soc.* 127:17421–28
57. Lewis PA, Inman CE, Yao YX, Tour JM, Hutchison JE, et al. 2004. Mediating stochastic switching of single molecules using chemical functionality. *J. Am. Chem. Soc.* 126:12214–15

58. Moore AM, Dameron AA, Mantooth BA, Smith RK, Fuchs DJ, et al. 2006. Molecular engineering and measurements to test hypothesized mechanisms in single molecule conductance switching. *J. Am. Chem. Soc.* 128:1959–67
59. Dameron AA, Ciszek JW, Tour JM, Weiss PS. 2004. Effect of hindered internal rotation on packing and conductance of self-assembled monolayers. *J. Phys. Chem. B* 108:16761–67
60. Bumm LA, Arnold JJ, Cygan MT, Dunbar TD, Burgin TP, et al. 1996. Are single molecular wires conducting? *Science* 271:1705–7
61. Sainoo Y, Kim Y, Okawa T, Komeda T, Shigekawa H, et al. 2005. Excitation of molecular vibrational modes with inelastic scanning tunneling microscopy processes: examination through action spectra of *cis*-2-butene on Pd(110). *Phys. Rev. Lett.* 95:246102
62. Kawai M, Komeda T, Kim Y, Sainoo Y, Katano S. 2004. Single-molecule reactions and spectroscopy via vibrational excitation. *Phil. Trans. R. Soc. Lond. A* 362:1163–71
63. Avouris P, Lyo IW. 1991. Probing and inducing surface chemistry on the atomic scale using the STM. *Am. Inst. Phys. Conf. Proc.* 241:283–97
64. Stroscio JA, Feenstra RM, Fein AP. 1986. Electronic structure of the Si(111)-2×1 surface by scanning tunneling microscopy. *Phys. Rev. Lett.* 57:2579–82
65. Avouris P, Lyo IW. 1991. Probing and inducing surface chemistry with the STM: the reactions of Si(111)-7×7 with H_2O and O_2. *Surf. Sci.* 242:1–11
66. Lyo IW, Avouris P. 1989. Negative differential resistance on the atomic scale: implications for atomic scale devices. *Science* 245:1369–71
67. Bedrossian P, Chen DM, Mortensen K, Golovchenko J. 1989. Demonstration of the tunnel-diode effect on an atomic scale. *Nature* 342:258–60
68. Feenstra RM. 1989. Electronic states of metal atoms on the GaAs(110) surface studied by scanning tunneling microscopy. *Phys. Rev. Lett.* 63:1412–15
69. Lang ND. 1986. Spectroscopy of single atoms in the scanning tunneling microscope. *Phys. Rev. B* 34:5947–50
70. Crommie MF, Lutz CP, Eigler DM. 1993. Spectroscopy of a single adsorbed atom. *Phys. Rev. B* 48:2851–54
71. Stipe BC, Rezaei MA, Ho W. 1998. Single-molecule vibrational spectroscopy and microscopy. *Science* 280:1732–35
72. Lee HJ, Ho W. 2000. Structural determination by single-molecule vibrational spectroscopy and microscopy: contrast between copper and iron carbonyls. *Phys. Rev. B* 61:R16347–50
73. Pascual JI, Jackiw JJ, Song Z, Weiss PS, Conrad H, et al. 2001. Adsorbate-substrate vibrational modes of benzene on Ag(110) resolved with scanning tunneling spectroscopy. *Phys. Rev. Lett.* 86:1050–53
74. Ferris JH, Kushmerick JG, Johnson JA, Yoshikawa Youngquist MG, Kessinger RB, et al. 1998. Design, operation, and housing of an ultrastable, low-temperature, ultrahigh vacuum scanning tunneling microscope. *Rev. Sci. Instrum.* 69:2691–95
75. Stipe BC, Rezaei MA, Ho W. 1998. Coupling of vibrational excitation to the rotational motion of a single adsorbed molecule. *Phys. Rev. Lett.* 81:1263–66

76. Lauhon LJ, Ho W. 1999. Single-molecule vibrational spectroscopy and microscopy: CO on Cu(001) and Cu(110). *Phys. Rev. B* 60:R8525–28
77. Moresco F, Meyer G, Rieder KH. 1999. Vibrational spectroscopy of CO/Cu(211) with a CO terminated tip. *Mod. Phys. Lett. B* 13:709–15
78. Heinrich AJ, Gupta JA, Lutz CP, Eigler DM. 2004. Single-atom spin-flip spectroscopy. *Science* 306:466–69
79. Hirjibehedin CF, Lutz CP, Heinrich AJ. 2006. Spin coupling in engineered atomic structures. *Science* 312:1021–24
80. Hirjibehedin CF, Lin C-Y, Otte AF, Ternes M, Lutz CP, et al. 2007. Large magnetic anisotropy of a single atomic spin embedded in a surface molecular network. *Science* 317:1199–203
81. Blum AS, Yang JC, Shashidhar R, Ratna BR. 2003. Comparing the conductivity of molecular wires with the scanning tunneling microscope. *Appl. Phys. Lett.* 82:3322–24
82. Kushmerick JG, Holt DB, Pollack SK, Ratner MA, Yang JC, et al. 2002. Effect of bond-length alternation in molecular wires. *J. Am. Chem. Soc.* 124:10654–55
83. Kushmerick JG, Naciri J, Yang JC, Shashidhar R. 2003. Conductance scaling of molecular wires in parallel. *Nano Lett.* 3:897–900
84. Kushmerick JG, Allara DL, Mallouk TE, Mayer TS. 2004. Electrical and spectroscopic characterization of molecular junctions. *MRS Bull.* 29:396–402
85. Sikes HD, Smalley JF, Dudek SP, Cook AR, Newton MD, et al. 2001. Rapid electron tunneling through oligophenylenevinylene bridges. *Science* 291:1519–23
86. Dudek SP, Sikes HD, Chidsey CED. 2001. Synthesis of ferrocenethiols containing oligo(phenylenevinylene) bridges and their characterization on gold electrodes. *J. Am. Chem. Soc.* 123:8033–38
87. Sachs SB, Dudek SP, Hsung RP, Sita LR, Smalley JF, et al. 1997. Rates of interfacial electron transfer through π-conjugated spacers. *J. Am. Chem. Soc.* 119:10563–64
88. Simon U. 1998. Charge transport in nanoparticle arrangements. *Adv. Mater.* 10:1487–92
89. Smith RK, Nanayakkara SU, Woehrle GH, Pearl TP, Blake MM, et al. 2006. Spectral diffusion in the tunneling spectra of ligand-stabilized undecagold clusters. *J. Am. Chem. Soc.* 128:9266–67
90. Wang B, Wang H, Li H, Zeng C, Hou JG, et al. 2001. Tunable single-electron tunneling behavior of ligand-stabilized gold particles on self-assembled monolayers. *Phys. Rev. B* 63:035403
91. Xue YQ, Ratner MA. 2003. Microscopic theory of single-electron tunneling through molecular-assembled metallic nanoparticles. *Phys. Rev. B* 68:235410
92. Zhang HJ, Schmid G, Hartmann U. 2003. Reduced metallic properties of ligand-stabilized small metal clusters. *Nano Lett.* 3:305–7
93. Andres RP, Bein T, Dorogi M, Feng S, Henderson JI, et al. 1996. 'Coulomb staircase' at room temperature in a self-assembled molecular nanostructure. *Science* 272:1323–25

94. Dorogi M, Gomez J, Osifchin R, Andres RP, Reifenberger R. 1995. Room-temperature Coulomb blockade from a self-assembled molecular nanostructure. *Phys. Rev. B* 52:9071–77
95. Andres RP, Datta S, Dorogi M, Gomez J, Henderson JI, et al. 1996. Room temperature Coulomb blockade and Coulomb staircase from self-assembled nanostructures. *J. Vac. Sci. Technol. A* 14:1178–83
96. Einstein TL, Schrieffer JR. 1973. Indirect interaction between adatoms on a tight-binding solid. *Phys. Rev. B* 7:3629–48
97. Tsong TT. 1973. Field-ion microscope observations of indirect interaction between adatoms on metal surfaces. *Phys. Rev. Lett.* 31:1207–11
98. Watanabe F, Ehrlich G. 1989. Direct mapping of adatom-adatom interactions. *Phys. Rev. Lett.* 62:1146–49
99. Crommie MF, Lutz CP, Eigler DM. 1993. Imaging standing waves in a two-dimensional electron gas. *Nature* 363:524–27
100. Gartland PO, Slagsvold BJ. 1975. Transitions conserving parallel momentum in photoemission from the (111) face of copper. *Phys. Rev. B* 12:4047–58
101. Memmel N. 1998. Monitoring and modifying properties of metal surfaces by electronic surface states. *Surf. Sci. Rep.* 32:91–163
102. Kamna MM, Stranick SJ, Weiss PS. 1996. Imaging substrate-mediated interactions. *Science* 274:118–19
103. Merrick ML, Luo WW, Fichthorn KA. 2003. Substrate-mediated interactions on solid surfaces: theory, experiment, and consequences for thin-film morphology. *Prog. Surf. Sci.* 72:117–34
104. Nanayakkara SU, Sykes ECH, Fernández-Torres LC, Blake MM, Weiss PS. 2007. Long-range electronic interactions at high temperature: bromine adatom islands on Cu(111). *Phys. Rev. Lett.* 98:206108
105. Stranick SJ, Kamna MM, Weiss PS. 1995. Interactions and dynamics of benzene on Cu{111} at low temperature. *Surf. Sci.* 338:41–59
106. Silly F, Pivetta M, Ternes M, Patthey F, Pelz JP, et al. 2004. Creation of an atomic superlattice by immersing metallic adatoms in a two-dimensional electron sea. *Phys. Rev. Lett.* 92:01610
107. Wahlström E, Ekvall I, Olin H, Wallden L. 1998. Long-range interaction between adatoms at the Cu(111) surface imaged by scanning tunnelling microscopy. *Appl. Phys. A* 66:S1107–10
108. Kulawik M, Rust H-P, Heyde M, Mantooth BA, Weiss PS. 2005. Interaction of CO molecules with surface state electrons on Ag{111}. *Surf. Sci.* 590:L253–58
109. Repp J, Moresco F, Meyer G, Rieder KH, Hyldgaard P, et al. 2000. Substrate mediated long-range oscillatory interaction between adatoms: Cu/Cu(111). *Phys. Rev. Lett.* 85:2981–84
110. Knorr N, Brune H, Epple M, Hirstein A, Schneider MA, et al. 2002. Long-range adsorbate interactions mediated by a two-dimensional electron gas. *Phys. Rev. B* 65:115420–21
111. Smoluchowski R. 1941. Anisotrophy of the electronic work function of metals. *Phys. Rev.* 60:661–74
112. Crommie MF, Lutz CP, Eigler DM. 1993. Confinement of electrons to quantum corrals on a metal surface. *Science* 262:218–20

113. Hasegawa Y, Avouris P. 1993. Direct observation of standing-wave formation at surface steps using scanning tunneling spectroscopy. *Phys. Rev. Lett.* 71:1071–74
114. Avouris P, Lyo IW, Molinás-Mata P. 1995. STM studies of the interaction of surface-state electrons on metals with steps and adsorbates. *Chem. Phys. Lett.* 240:423–28
115. Lau KH, Kohn W. 1978. Indirect long-range oscillatory interaction between adsorbed atoms. *Surf. Sci.* 75:69–85
116. Fujita D, Amemiya K, Yakabe T, Nejoh H, Sato T, et al. 1997. Anisotropic standing-wave formation on an Au(111)-($23 \times \sqrt{3}$) reconstructed surface. *Phys. Rev. Lett.* 78:3904–7
117. Jeandupeux O, Burgi L, Hirstein A, Brune H, Kern K. 1999. Thermal damping of quantum interference patterns of surface-state electrons. *Phys. Rev. B* 59:15926–34
118. Pascual JI, Jackiw JJ, Kelly KF, Conrad H, Rust H-P, et al. 2000. Local electronic structural effects and measurements on the adsorption of benzene on Ag(110). *Phys. Rev. B* 62:12632–35
119. Weiss PS, Kamna MM, Graham TM, Stranick SJ. 1998. Imaging benzene molecules and phenyl radicals on Cu{111}. *Langmuir* 14:1284–89
120. Sautet P, Bocquet ML. 1994. A theoretical analysis of the site dependence of the shape of a molecule in STM images. *Surf. Sci.* 304:L445–L50
121. Sykes ECH, Mantooth BA, Han P, Donhauser ZJ, Weiss PS. 2005. Substrate-mediated intermolecular interactions: a quantitative single molecule analysis. *J. Am. Chem. Soc.* 127:7255–60
122. Pascual JI, Jackiw JJ, Song Z, Weiss PS, Conrad H, et al. 2002. Adsorption and growth of benzene on Ag(110). *Surf. Sci.* 502:1–6
123. Urbach LE, Percival KL, Hicks JM, Plummer EW, Dai HL. 1992. Resonant surface 2nd harmonic generation: surface-states on Ag(110). *Phys. Rev. B* 45:3769–72
124. Ullmann F, Bielecki J. 1901. Über Synthesen in der Biphenylreihe. *Ber. Dtsch. Chem. Ges.* 34:2174–85
125. Hla SW, Bartels L, Meyer G, Rieder K-H. 2000. Inducing all steps of a chemical reaction with the scanning tunneling microscope tip: towards single molecule engineering. *Phys. Rev. Lett.* 85:2777–80
126. Grafström S. 2002. Photoassisted scanning tunneling microscopy. *Appl. Phys. Rev.* 91:1717–53
127. Stranick SJ, Weiss PS, Parikh AN, Allara DL. 1993. Alternating current scanning tunneling spectroscopy of self-assembled monolayers on gold. *J. Vac. Sci. Technol. A* 11:739–41
128. Stranick SJ, Weiss PS. 1994. Alternating current scanning tunneling microscopy and nonlinear spectroscopy. *J. Phys. Chem.* 98:1762–64
129. Stranick SJ, Weiss PS. 1994. A tunable microwave frequency alternating-current scanning tunneling microscope. *Rev. Sci. Instrum.* 65:918–21
130. Bumm LA, Weiss PS. 1995. Small cavity nonresonant tunable microwave frequency alternating current scanning tunneling microscope. *Rev. Sci. Instrum.* 66:4140–45